Defective Carbon–CoP Nanoparticles Hybrids with Interfacial Charges Polarization for Efficient Bifunctional Oxygen Electrocatalysis

Yunxiang Lin, Li Yang, Youkui Zhang, Hongliang Jiang, Zijian Xiao, Chuanqiang Wu, Guobin Zhang, Jun Jiang, and Li Song**

The development of efficient catalysts for both oxygen reduction and evolution reactions (oxygen reduction reaction (ORR) and oxygen evolution reaction (OER)) is central to regenerative fuel cells and rechargeable metal–air batteries. It is highly desirable to achieve the efficient integration of dual active components into the catalysts and to understand the interaction between the dual components. Here, a facile approach is demonstrated to construct defective carbon–CoP nanoparticle hybrids as bifunctional oxygen electrocatalysts, and further probe the interfacial charge distribution behavior. By combining multiple synchrotron-based X-ray spectroscopic characterizations with density functional theory calculations, the interfacial charge polarization with the electrons gathering at the defective carbon surface and the holes gathering at the CoP surface due to strong interfacial coupling is revealed, which simultaneously facilitates the ORR and OER with remarkable bifunctional oxygen electrode activities. This work not only offers a bifunctional oxygen catalyst with outstanding performance, but also unravels the promoting factor of the hybrids from the view of interfacial charge distribution.

Oxygen reduction reaction (ORR) and oxygen evolution reaction (OER) have been widely studied due to their extensive applications in energy conversion and storage.[1–10] However, the complicated multielectron transfer processes and high energy barrier of activating reactant lead to a high overpotential to drive the ORR and OER. Although noble-metal (e.g., Ruthenium, Iridium, and Platinum) based materials have shown

Y. Lin, Dr. L. Yang, Y. Zhang, Dr. H. Jiang, Z. Xiao, C. Wu, Prof. G. Zhang, Prof. J. Jiang, Prof. L. Song
National Synchrotron Radiation Laboratory
CAS Center for Excellence in Nanoscience
Hefei National Laboratory for Physical Sciences at the Microscale
iChEM (Collaborative Innovation Center of Chemistry for Energy Materials) School of Chemistry and Materials Science
University of Science and Technology of China
Hefei 230026, P. R. China
E-mail: jhlworld@ustc.edu.cn; song2012@ustc.edu.cn
Y. Zhang
School of National Defense Science and Technology
Southwest University of Science and Technology
Mianyang 621010, China

The ORCID identification number(s) for the author(s) of this article can be found under https://doi.org/10.1002/aenm.201703623.

ideal performance toward ORR or OER, the high price, scarcity, and instability still hampers their large-scale generalization. At present, developing efficient and non-noble-metal catalysts has attracted extensive interest.[11–18]

For ORR, defective carbon-based materials, typically heteroatom-doped carbon, are extensively demonstrated as efficient electrocatalysts.[19–22] For OER, in addition to common transition metal oxides or (oxy)hydroxides, transition metal phosphides (TMPs) have achieved considerable research and development attention due to superior performance.[23–27] In this regard, the composites of the TMPs and defective carbon are considered as promising candidates for both ORR and OER. More recently, some works reported that the composites of the TMPs and defective carbon compared to the single component displayed enhanced catalytic performance, which was probably attributed to the increased electronic conductivity due to the introduction of conductive carbon.[28–30] However, the promoting factor was not well understood. For the composites, undoubtedly, the interfacial properties, especially the interfacial charge states, are important parameters that could influence the catalytic performance.[31,32] Therefore, in order to overcome high catalytic reaction barrier, designing the hybrids of the TMPs and defective carbon and probing the interfacial charge distribution behavior are highly desirable to realize bifunctional oxygen electrocatalysis.

Herein, we constructed a new type of hybrids of the CoP and defective carbon (marked as CoP–DC). We revealed the interfacial charge transfer process of the hybrids by multiple synchrotron-based X-ray absorption structure, ultraviolet photoelectron spectra (UPS), X-ray photoelectron spectroscopy (XPS), and density functional theory (DFT) calculations. The interfacial charge redistribution was observed, which subsequently contributed to enhanced ORR activity on the defective carbon and enhanced OER activity on the CoP.

The CoP–DC hybrids were synthesized through a simple phosphorization reaction toward the Co^{2+}-contained polymer hydrogel. Typically, the polymer hydrogel was obtained by inserting Co^{2+} into polymer hydrogel framework under alkaline condition according to previous reports, and then was phosphorized

**ADVANCED
SCIENCE NEWS**
www.advancedsciencenews.com

**ADVANCED
ENERGY
MATERIALS**
www.advenergymat.de

by nontoxic red phosphorus under N_2 flow at 900 °C (see Supporting Information for details). For comparison, the DC and the Co nanoparticles-contained DC (Co–DC) were also obtained under the similar condition without the addition of Co ion and red phosphorus, respectively. X-ray diffraction (XRD) was carried out to investigate the crystal structure of CoP–DC and the control samples. As shown in **Figure 1**a, XRD pattern of the DC sample shows wide peak at 26°, suggesting the typical defective structure with low long-range order. The metallic Co peaks for Co–DC at 44° and 51°, indicating that the Co ion has been reduced to metallic Co during the anneal process under N_2 flow at 900 °C. For the CoP–DC, a series peaks at 31.6°, 35.3°, 36.3°, 46.2°, 48.1°, 52.3°, and 56.0° can be assigned to the (011), (200), (111), (112), (211), (103), and (301) lattice planes of CoP (JCPDS: 29–0497), respectively, indicating the CoP component inside the obtained samples. The Raman spectra (Figure S1, Supporting Information) of CoP–DC and DC show two dominant peaks at 1340 and 1590 cm^{-1} corresponding to the D and G band, respectively. Comparing to that of pure DC, the intensity ratio (I_D/I_G) of D and G band decreased in CoP–DC and Co–DC samples due to the graphitization during anneal process,

implying the well interfacial contact between the CoP or Co nanoparticles and DC. Co–DC exhibited the lowest I_D/I_G ratio indicating the much lower defects density in Co–DC.[33,34] To further probe the microstructure, transmission electron microscopy (TEM) and high-resolution TEM (HRTEM) images of CoP–DC were performed, showing that the CoP nanoparticles (average diameter of 30 nm) were uniformly embedded into the DC to form core–shell structure (Figure 1b,c). Besides, CoP nanoparticles in CoP–DC show the similar sizes comparing to Co nanoparticles in Co–DC (Figure S2a, Supporting Information), which means that the phosphorization had no influence on the size of nanoparticles during the anneal process (Figure S2b,c, Supporting Information). Furthermore, the CoP nanoparticles in the CoP–DC show continuous and ordered lattice fringes with the lattice spacings of 2.47 and 3.75 Å and the crystal plane angle of 86.4° (Figure S3, Supporting Information), which correspond to the (11$\bar{1}$) and (101) planes, respectively, according to the lattice parameters of the CoP (JCPDS 29–0497). Notably, the carbon layers around the CoP display typical curved lattice fringes, revealing the defective structure. Thermogravimetric analysis (TGA) of CoP–DC and HNO_3-treated CoP–DC (see Supporting Information for details) were conducted to explore the defective features. The mass fraction of CoP nanoparticles in DC–CoP was calculated to be 57.32%, while the value decreased to 11.42% in the HNO_3-treated CoP–DC, indicating that ≈80% of CoP nanoparticles in CoP–DC were not fully encased by the carbon. The above TEM observation and TGA results further reveal that the carbon layers exhibit abundant structural defects, displaying the typical interfacial structure with the exposure of dual components (As shown in Figure 1e, the dotted circle means the defective carbon sites).
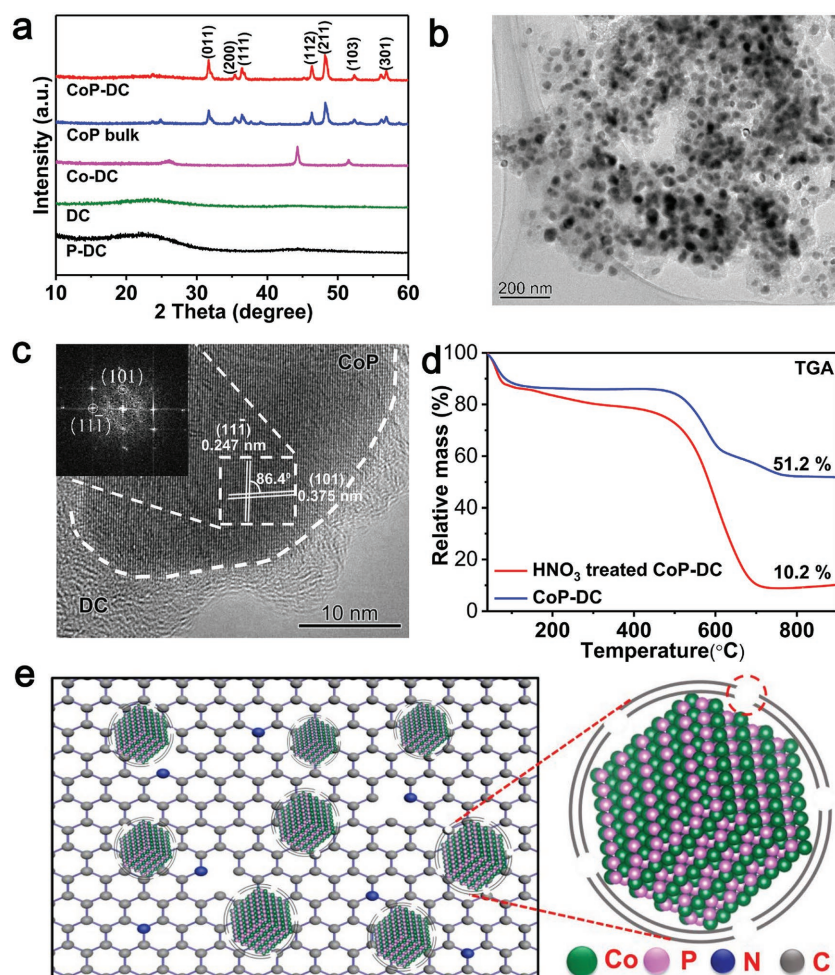
To investigate the electronic structure of the CoP–DC, soft X-ray absorption near-edge structure (XANES) measurement was used to detect the L-edge excitation of elemental Co and K-edge excitation of elemental C (**Figure 2**a,b). As can be seen from Figure 2a, two separated peaks of Co L-edge XANES spectra at around 777 and 792 eV are assigned to the L_3 and L_2 edges of core electrons transition from $2p_{3/2}$ and $2p_{1/2}$ hybrid orbit to P 3p orbit level, respectively. The different intensity of the absorption peaks is mainly caused by the different vacancies of unoccupied states of Co sites. Comparing to CoP bulk, the CoP–DC own stronger L_3 intensity, indicating that more vacancies existed in Co 3d states of CoP–DC, probably due to the electron transfer from the Co sites to C sites.[35,36] To further verify this, the C K-edge spectra was analyzed. From Figure 2b, the absorption peak A at 284 eV responds to π^* structure and peak D at 291 eV responds to σ^* structure of C−C bonds, respectively. In addition, we also observed

Figure 1. a) XRD of the CoP–DC and control samples. b) TEM and c) HRTEM images of the CoP–DC. d) TGA of CoP–DC sample and HNO_3-treated CoP–DC sample. e) Diagrammatic drawing of the morphology structure for the CoP–DC.
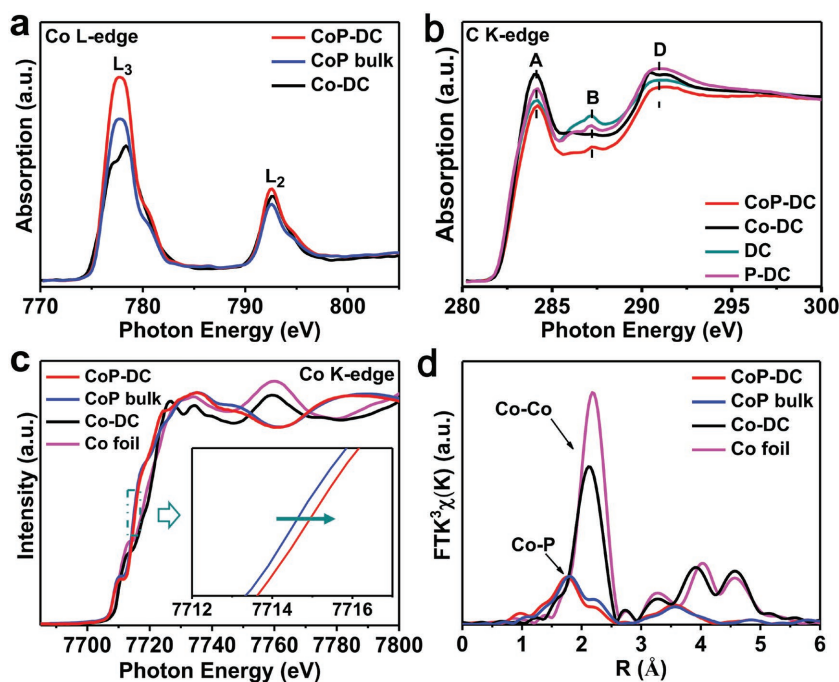
Figure 2. Normalized a) Co L-edge, b) C K-edge, c) Co K-edge XANES spectra for the CoP–DC and other contrast samples. d) The corresponding k^3-weighted $\chi(k)$-function of the Co K-edge EXAFS spectra.

the peaks (marked as peak B) between π^* and σ^* owing to the sp^3 hybrid bonds between C and other functional-groups such as C=O and C—O (COOH).[37–39] The DC sample shows the strongest peak B, indicating the most sp^3 hybrid bonds between C and other functional-groups than other samples. For the Co–DC and CoP–DC, the intensity of the peak B significantly decreased, which can be attributed to the catalytic graphitization of the Co and CoP during heating process. The intensity of peak B for the Co–DC is slightly weaker than that of CoP–DC, indicating that the less defects in the DC framework of Co–DC, which can be also observed from Raman spectra mentioned above. Notably, the intensity of peak A and D for the CoP–DC is the weakest, indicating the strongest electrons coupling and most electron transfer from the Co sites to C sites.[37,40,41] This result is in good agreement with XPS analysis (Figure S4, Supporting Information). Moreover, the P L-edge spectrum for the CoP–DC shows a peak B at 142 eV, while the peak is disappeared for the CoP bulk, further indicating the strong interfacial interaction between CoP and C (Figure S5, Supporting Information).[42,43] X-ray absorption fine structure (XAFS) was performed to figure out the local structure of CoP–DC, CoP bulk and Co–DC (Figure 2c). There is no obvious distinction between CoP–DC and CoP bulk, meaning that the existence of the standard CoP framework in both samples. As displayed in the inset of Figure 2c, a shift of absorption threshold to high energy is observed after the CoP coupled with defective carbon, indicating the electron transfer from the CoP core to defective carbon shell.[44,45] This result is also consistent with XPS, Co L-edge, and C K-edge XANES spectra as discussed above. Extended X-ray absorption fine structure (EXAFS) method at Co K-edge absorption was also employed to investigate the

geometry structure of CoP–DC and Co–DC by using CoP bulk and Co foil as reference samples (Figure 2d). As shown in the Figure 2d, two main peaks at the R space ranging from 1 to 3 Å are presented, in which the prepeak (1.78 Å) and the postpeak (2.15 Å) are corresponding to the Co—P and Co—Co bond, respectively. It is easy to point out that both the Co—P and Co—Co bonds in CoP–DC and Co–DC samples are slightly shifted to low-R with relatively weak peak intensity, which is caused by the surface structural disorder due to the intimate interfacial contact in the hybrids.[46,47] Insights into the coordination structure of CoP–DC and its contrast samples by fitting in the R-space of the first coordination shell further support the structural disorder (Figure S6, Table S1, Supporting Information).

To further understand the interfacial charge redistribution, secondary electron cut-off (SECO) regions of UPS were applied to calculate the work function (Φ) of materials.[48] Normalized SECO spectra and calculated Φ of CoP bulk, DC, and CoP–DC are exhibited in **Figure 3**a,b. Clearly, the CoP–DC shows the smallest Φ (4.3 eV) among these samples, while the Φ of DC and CoP bulk are 5.2 and 4.7 eV, respectively. According to previous reports, the lowest Φ suggest that the CoP–DC offers the smallest energy barrier for extracting electron from the CoP–DC surface, thereby promoting the reduction process, typically ORR.[49,50] First-principles calculations (see the Supporting Information for details) were also performed to understand the interfacial charge behavior of the CoP–DC interfacial structure. Differential charge density of the CoP–DC hybrids shows that electrons would migrate from CoP to DC layer due to the strong interfacial polarization between each other (Figure 3c). As a result, DC surface would collect electrons while CoP accumulate positive charges (holes), inducing the electron separation and hole distribution. Bader charge analysis further found that 1.30 electrons could gather at the outer DC surface. This electron accumulation would be beneficial to the following ORR on the defective carbon. Besides, it is well documented that the holes collection at the CoP could promote the formation of true catalytically active sites (CoOOH) for OER,[51,52] thereby boosting the OER performance. As such, the interfacial charge redistribution on the CoP–DC interfacial structure would simultaneously facilitate the ORR and OER.

In order to evaluate the expected bifunctional performance of the designed CoP–DC hybrids, both the ORR and OER measurements were carried on rotating disk electrode (RDE) and rotating RDE (RRDE) in 0.1 M KOH solution (**Figure 4**). Cyclic voltammetry (CV) curves for CoP–DC (Figure 4a) shows no featured peak for cathodic current in N_2-saturated KOH electrolyte within the potential range from −0.02 to 1.02 V (vs RHE), while an obvious oxygen reduction peak at 0.74 V in O_2-saturated KOH electrolyte is presented, suggesting a distinct oxygen reduction activity for CoP–DC. Liner sweep voltammetry

ADVANCED
SCIENCE NEWS
www.advancedsciencenews.com

ADVANCED
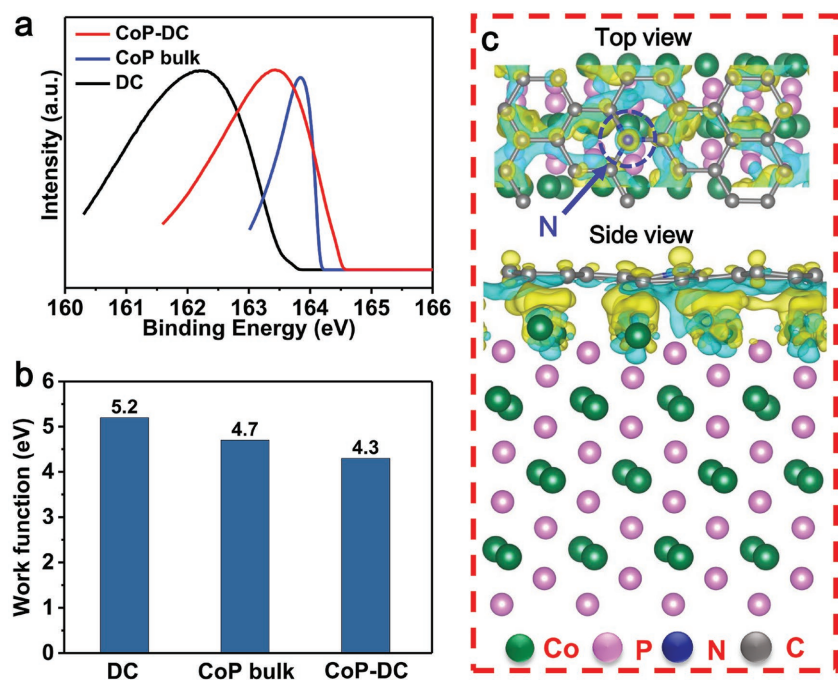**ENERGY**
MATERIALS
www.advenergymat.de

Figure 3. a) SECO regions of UPS spectra and b) work functions for CoP–DC, CoP bulk and DC. c,d) The computed differential charge density between CoP and NC from top and side views. Yellow and blue bubbles separately represent the electron and hole charges with the isovalue of 0.0035 e $Å^{-3}$.

(LSV) curves of all the as-prepared samples under rotating rates of 1600 rpm were further measured to compare the ORR performance (Figure 4b). Strikingly, CoP–DC shows the nearest onset potential comparing to commercial Pt/C and the half-wave potential (0.81 V vs RHE) is slightly lower than that of Pt/C (0.85 V vs RHE), indicating the excellent ORR performance of CoP–DC. The understanding of ORR mechanism is recorded from LSV curves under various rotation speed range from 225 to 2025 rpm with a scan rate of 10 mV s^{-1} (Figures S7 and S8, Supporting Information). The J_L increased with the rotating speed increasing own to the shortened diffusion distance at high rotating speeds and enhanced mass transport at the electrode surface.[53,54] The Koutecky–Levich (K–L) plots express pretty good linearity and parallelism, indicating the first-order reaction kinetics toward the dissolved oxygen. Electron transfer number (n) and the formation of peroxide species (HO_2^-) were calculated from RRDE measurement at a rotation speed of 1600 rpm. The values of n are 3.40, 3.45, 3.49, 3.80, and 3.82 for P–DC, DC, CoP bulk, Co–DC, and CoP–DC over a potential range from 0.2 to 0.8 V (vs RHE), respectively, and the percentage of peroxide species for CoP–DC is 16%, indicating a near four-electron ORR pathway in case of CoP–DC (Figure 4c; Figure S9, Supporting Information). Previous work verified that Co—N bond showed remarkable effect in ORR.[5,54] In order to eliminate the contribution of Co—N bonds which derived from the nitrogenous precursor (Figure S4d, Supporting Information), the CoP–DC was first dipped in 10×10^{-3} M KSCN solution for 60 min to restrain the catalytic activity of Co—N species and then tested in 0.1 M KOH for ORR.[55,56] As shown in Figure S10 of the Supporting Information, LSV

curves of CoP–DC and KSCN treated CoP–DC show ignorable difference, indicating the ORR performance was mainly contributed by the synergistic effect of CoP and DC rather than Co—N bonds.[57–60] Comparing the LSV curves of CoP–DC with that of Co–DC, the higher ORR activity indicates that the phosphorization plays a non-negligible role in the ORR process. As discussed in the above X-ray absorption spectra, the stronger interfacial electrons coupling of the CoP–DC compared to that of the Co–DC leads to the lower work function of the CoP–DC, which offers the smaller energy barrier for extracting electron from the CoP–DC surface and thereby promote the ORR process. Besides, the half-wave potential shows slightly negative shift about 8 mV after durability test under CV test for 5000 circles (Figure S11, Supporting Information), indicating a good stability for CoP–DC toward ORR.

Our catalysts were also explored for electrocatalytic OER in 0.1 M KOH solution. As shown in Figure 4d, an overpotential of 0.32 V is required to obtain the current density of 10 mV cm^{-2} for CoP–DC, which is equal to IrO_2 and much smaller than that of other contrast samples. Meanwhile, Tafel slopes of all the samples were calculated from LSV curves to estimate the reaction kinetics toward OER (Figure 4e). Impressively, the CoP–DC shows a smallest value of Tafel slope (52.5 mV dec^{-1}) among all the as-prepared samples and even better than that of IrO_2, which means CoP–DC performing a better electron transfer efficiency. Electrochemical active surface areas were further measured by CV testing at different scan rate from 20 to 120 mV s^{-1} to deep understand the active surface area of these as-obtained catalysts (Figure S12, Supporting Information). The CoP–DC shows highest double-layered capacitance (C_{dl}) of 26.98 mF cm^{-2}, indicating the largest active surface area, which offers more active sites during electrocatalytic process. Moreover, the CoP–DC also shows an ideal stability during the long time (20 h) test in 0.1 M KOH at a constant current density of 10 mA cm^{-2} (Figure S13, Supporting Information). As discussed above, the high density of holes on the CoP nanoparticles is definitely beneficial to OER process. According to previous significant reports,[51,52] O-doped CoP and carbon supported metal hydroxides, typical hole-doped catalysts, show significantly enhanced OER activities. In the two studies, DFT calculations and experimental results strongly indicate the promoted conversion from the metal phosphides or metal hydroxides to the related oxyhydroxides. The oxyhydroxides are generally considered as actually active sites for OER.[61,62] Thus, the high density of holes on the CoP nanoparticles would promote the generation of Co-based oxyhydroxides and thereby boost the activities. More importantly, the overall electrocatalytic activities of all the samples were investigated (Figure 4f) at the current density of 10 mA cm^{-2} for OER and −3 mA cm^{-2} for ORR (Table S2, Supporting Information). Notably, a lowest oxygen electrode
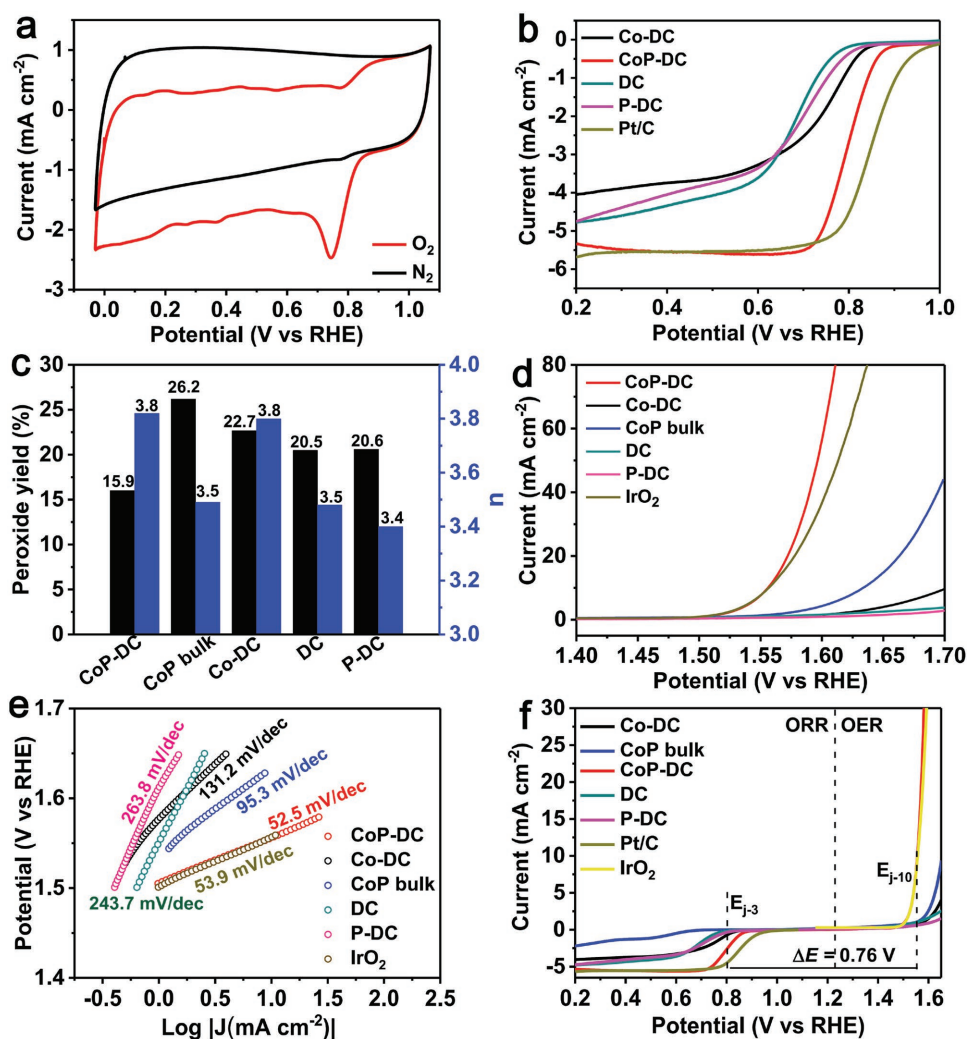
**ADVANCED
SCIENCE NEWS**
www.advancedsciencenews.com

**ADVANCED
ENERGY
MATERIALS**
www.advenergymat.de

Figure 4. a) CV curves of CoP–DC in N_2 and O_2 saturated 0.1 M KOH electrolyte. b) ORR LSV carves of as-prepared CoP–DC, Co–DC, DC, P–DC, and Pt/C in O_2-saturated 0.1 M KOH electrolyte at a rotation speed of 1600 rpm with a scan rate of 10 mV s^{-1}. c) Peroxide yield (black) and electron transfer number (n) (blue) of as-prepared CoP–DC, CoP bulk, Co–DC DC, and P–DC calculated from RRDE voltammograms. d) OER LSV carves and e) corresponding Tafel plots for CoP–DC, Co–DC, CoP bulk DC P–DC, and IrO_2. f) The overall LSV curves of all samples in the whole ORR and OER region in 0.1 M KOH.

activity (ΔE) of CoP–DC obtained 0.76 V, indicating that CoP–DC owns excellent bifunctional performance, which is comparable to the recent works (Table S3, Supporting Information).

When decorating DC with CoP nanoparticles, the redistributed electrons and holes result in the high density of electrons gathered on the surface of DC and high density of holes gathered on CoP nanoparticles. Previous studies had revealed that the brilliant ORR activity of carbon-based materials mainly contributed by the large surface area, multiple active sites and high reduction states. As discussed above, the excellent bifunctional electrical performance of CoP–DC hybrids primary caused by the following aspects: (1) DC, with large surface area, has provided multiple active sites that made contribution to molecule capture; (2) the hybrids demonstrated a lowest Φ after CoP embedded into DC framework, thus decreased the reaction energy barrier;[49,63] (3) interfacial polarized electrons accumulated at the surface of DC was supposed to enhance the ORR while the holes accumulated at the CoP nanoparticles was a key factor in OER; (4) high density of electrons and holes promoted the speed of immediate product rebuilt on the catalysts surface, leading to the enhanced electrocatalytic performance.[54,64]

In summary, we developed the hybrids of CoP and defective carbon for efficient bifunctional oxygen electrocatalysis. We provided complete evidence that the interfacial charge redistribution occurred at the interface of CoP and defective carbon. Electrochemical tests suggested that the CoP–DC hybrids exhibited better ORR and OER activities comparing to the single component, indicating the key roles of the interfacial charge redistribution. The hybrids here have the potential for the application to promote the development of related energy technologies and devices. More importantly, the concept demonstrated here calls for future efforts on interfacial engineering for electrocatalysts design.

Supporting Information

Acknowledgements

Conflict of Interest

The authors declare no conflict of interest.

Keywords

[1] J. Suntivich, H. A. Gasteiger, N. Yabuuchi, H. Nakanishi, J. B. Goodenough, Y. Shao-Horn, *Nat. Chem.* **2011**, *3*, 546.
[2] Q. Li, R. Cao, J. Cho, G. Wu, *Adv. Energy Mater.* **2014**, *4*, 1301415.
[3] W. H. Niu, L. G. Li, X. J. Liu, N. Wang, J. Liu, W. J. Zhou, Z. H. Tang, S. W. Chen, *J. Am. Chem. Soc.* **2015**, *137*, 5555.
[4] M. K. Debe, *Nature* **2012**, *486*, 43.
[5] H.-F. Wang, C. Tang, B. Wang, B.-Q. Li, Q. Zhang, *Adv. Mater.* **2017**, *29*, 1702327.
[6] Q. Wang, L. Shang, R. Shi, X. Zhang, Y. Zhao, G. I. N. Waterhouse, L.-Z. Wu, C.-H. Tung, T. Zhang, *Adv. Energy Mater.* **2017**, *7*, 1700467.
[7] Y. Hou, T. Huang, Z. Wen, S. Mao, S. Cui, J. Chen, *Adv. Energy Mater.* **2014**, *4*, 1400337.
[8] Y. Liu, Y. Zhu, J. Shen, J. Huang, X. Yang, C. Li, *Nanoscale* **2018**, *10*, 2603.
[9] Y. Hao, Y. Xu, W. Liu, X. Sun, *Mater. Horiz.* **2018**, *5*, 108.
[10] H.-C. Li, Y.-J. Zhang, X. Hu, W.-J. Liu, J.-J. Chen, H.-Q. Yu, *Adv. Energy Mater.* **2018**, https://doi.org/10.1002/aenm.201702734.
[11] V. Petrykin, K. Macounova, O. Shlyakhtin, P. Krtil, *Angew. Chem.* **2010**, *122*, 4923; *Angew. Chem., Int. Ed.* **2010**, *49*, 4813.
[12] J. Su, Y. Yang, G. Xia, J. Chen, P. Jiang, Q. Chen, *Nat. Commun.* **2017**, *8*, 14969.
[13] X. Zou, Y. Zhang, *Chem. Soc. Rev.* **2015**, *44*, 5148.
[14] D. V. Esposito, S. T. Hunt, A. L. Stottlemyer, K. D. Dobson, B. E. McCandless, R. W. Birkmire, J. G. Chen, *Angew. Chem.* **2010**, *122*, 10055; *Angew. Chem., Int. Ed.* **2010**, *49*, 9859.
[15] Y. Zheng, Y. Jiao, Y. Zhu, Q. Cai, A. Vasileff, L. H. Li, Y. Han, Y. Chen, S.-Z. Qiao, *J. Am. Chem. Soc.* **2017**, *9*, 3336.
[16] C. Meng, T. Ling, T.-Y. Ma, H. Wang, Z. Hu, Y. Zhou, J. Mao, X.-W. Du, M. Jaroniec, S.-Z. Qiao, *Adv. Mater.* **2016**, *29*, 1604607.
[17] B. Bayatsarmadi, Y. Zheng, A. Vasileff, S.-Z. Qiao, *Small* **2017**, *13*, 1700191.
[18] T. Ling, D.-Y. Yan, Y. Jiao, H. Wang, Y. Zheng, X. Zheng, J. Mao, X.-W. Du, Z. Hu, M. Jaroniec, S.-Z. Qiao, *Nat. Commun.* **2016**, *7*, 12876.
[19] Y. Li, W. Zhou, H. Wang, L. Xie, Y. Liang, F. Wei, J.-C. Idrobo, S. J. Pennycook, H. Dai, *Nat. Nanotechnol.* **2012**, *7*, 394.
[20] K. Waki, R. A. Wong, H. S. Oktaviano, T. Fujio, T. Nagai, K. Kimoto, K. Yamada, *Energy Environ. Sci.* **2014**, *7*, 1950.
[21] Y. Jiang, L. Yang, T. Sun, J. Zhao, Z. Lyu, O. Zhuo, X. Wang, Q. Wu, J. Ma, Z. Hu, *ACS Catal.* **2015**, *5*, 6707.
[22] C. Tang, B. Wang, H.-F. Wang, Q. Zhang, *Adv. Mater.* **2017**, *29*, 1703185.
[23] A. B. Laursen, K. R. Patraju, M. J. Whitaker, M. Retuerto, T. Sarkar, N. Yao, K. V. Ramanujachary, M. Greenblatt, G. C. Dismukes, *Energy Environ. Sci.* **2015**, *8*, 1027.
[24] W. Li, X. Gao, D. Xiong, F. Xia, J. Liu, W.-G. Song, J. Xu, S. M. Thalluri, M. F. Cerqueira, X. Fu, L. Liu, *Chem. Sci.* **2017**, *8*, 2952.
[25] J. Tian, Q. Liu, A. M. Asiri, X. Sun, *J. Am. Chem. Soc.* **2014**, *136*, 7587.
[26] W. Li, D. Xiong, X. Gao, W.-G. Song, F. Xia, L. Liu, *Catal. Today* **2017**, *287*, 122.
[27] L. Tian, X. Yan, X. Chen, L. Liu, X. Chen, *J. Mater. Chem. A* **2016**, *4*, 13011.
[28] Z. Pu, I. S. Amiinu, C. Zhang, M. Wang, Z. Kou, S. Mu, *Nanoscale* **2017**, *9*, 3555.
[29] Q. Liu, J. Tian, W. Cui, P. Jiang, N. Cheng, A. M. Asiri, X. Sun, *Angew. Chem.* **2014**, *126*, 6828; *Angew. Chem. Int. Ed.* **2014**, *53*, 6710.
[30] S. Han, Y. Feng, F. Zhang, C. Yang, Z. Yao, W. Zhao, F. Qiu, L. Yang, Y. Yao, X. Zhuang, X. Feng, *Adv. Funct. Mater.* **2015**, *25*, 3899.
[31] C. Guo, Y. Zheng, J. Ran, F. Xie, M. Jaroniec, S.-Z. Qiao, *Angew. Chem.* **2017**, *129*, 8659; *Angew. Chem., Int. Ed.* **2017**, *56*, 8539.
[32] G. G. Kumar, M. Christy, H. Jang, K. S. Nahm, *J. Power Sources* **2015**, *288*, 451.
[33] S. Peng, X. Han, L. Li, Z. Zhu, F. Cheng, M. Srinivansan, S. Adams, S. Ramakrishna, *Small* **2016**, *12*, 1359.
[34] I. Serrano-Esparza, J. Fan, J. M. Michalik, L. A. Rodríguez, M. R. Ibarra, J. M. de Teresa, *J. Phys. D: Appl. Phys.* **2016**, *49*, 105301.
[35] Y. Ma, N. Wassdahl, P. Skytt, J. Guo, J. Nordgren, P. D. Johnson, J.-E. Rubensson, T. Boske, W. Eberhardt, S. D. Kevan, *Phys. Rev. Lett.* **1992**, *69*, 2598.
[36] J. Zhong, H. Zhang, X. Sun, S.-T. Lee, *Adv. Mater.* **2014**, *26*, 7786.
[37] J. Zhong, J.-J. Deng, B.-H. Mao, T. Xie, X.-H. Sun, Z.-G. Mou, C.-H. Hong, P. Yang, S.-D. Wang, *Carbon* **2012**, *50*, 335.
[38] C.-J. Chen, P.-T. Chen, M. Basu, K.-C. Yang, Y.-R. Lu, C.-L. Dong, C.-G. Ma, C.-C. Shen, S.-F. Hu, R.-S. Liu, *J. Mater. Chem. A* **2015**, *3*, 23466.
[39] J. Okabayashi, T. Koyama, M. Suzuki, M. Tsujikawa, M. Shirai, D. Chiba, *Sci. Rep.* **2017**, *7*, 46132.
[40] V. Lee, L. Whittaker, C. Jaye, K. M. Baroudi, D. A. Fischer, S. Banerjee, *Chem. Mater.* **2009**, *21*, 3905.
[41] D. Pacilé, M. Papagno, A. F. Rodríguez, M. Grioni, L. Papagno, Ç. Ö. Girit, J. C. Meyer, G. E. Begtrup, A. Zettl, *Phys. Rev. Lett.* **2008**, *101*, 066806.
[42] H. Demirkiran, Y. Hu, L. Zuin, N. Appathurai, P. B. Aswath, *Mater. Sci. Eng., C* **2011**, *31*, 134.

**ADVANCED
SCIENCE NEWS**

www.advancedsciencenews.com

**ADVANCED
ENERGY
MATERIALS**

www.advenergymat.de

[43] J. Kruse, P. Leinweber, K.-U. Eckhardt, F. Godlinski, Y. Hu, L. Zuin, *J. Synchrotron Radiat.* **2009**, *16*, 247.

[44] X. Zhu, X. Dou, J. Dai, X. An, Y. Guo, L. Zhang, S. Tao, J. Zhao, W. Chu, X. C. Zeng, C. Wu, Y. Xie, *Angew. Chem.* **2016**, *128*, 12653; *Angew. Chem., Int. Ed.* **2016**, *55*, 12465.

[45] Q. Liu, Q. Fang, W. Chu, Y. Wan, X. Li, W. Xu, M. Habib, S. Tao, Y. Zhou, D. Liu, T. Xiang, A. Khail, X. Wu, M. Chhowalla, P. M. Ajayan, L. Song, *Chem. Mater.* **2017**, *29*, 4738.

[46] W. Liu, L. Cao, W. Cheng, Y. Cao, X. Liu, W. Zhang, X. Mou, L. Jin, X. Zheng, W. Che, Q. Liu, T. Yao, S. Wei, *Angew. Chem.* **2017**, *129*, 9440; *Angew. Chem., Int. Ed.* **2017**, *56*, 9312.

[47] J. F. Callejas, C. G. Read, E. J. Popczun, J. M. McEnaney, R. E. Schaak, *Chem. Mater.* **2015**, *27*, 3769.

[48] H. B. Yang, J. Miao, S.-F. Hung, J. Chen, H. B. Tao, X. Wang, L. Zhang, R. Chen, J. Gao, H. M. Chen, L. Dai, B. Liu, *Sci. Adv.* **2016**, *2*, e1501122.

[49] X. Li, W. Liu, M. Zhang, Y. Zhong, Z. Weng, Y. Mi, Y. Zhou, M. Li, J. J. Cha, Z. Tang, H. Jiang, X. Li, H. Wang, *Nano Lett.* **2017**, *17*, 2057.

[50] D. H. Lee, W. J. Lee, W. J. Lee, S. O. Kim, Y.-H. Kim, *Phys. Rev. Lett.* **2011**, *106*, 175502.

[51] G. Zhang, G. Wang, Y. Liu, H. Liu, J. Qu, J. Li, *J. Am. Chem. Soc.* **2016**, *138*, 14686.

[52] M. Görlin, J. Ferreira de Araújo, H. Schmies, D. Bernsmeier, S. Dresp, M. Gliech, Z. Jusys, P. Chernev, R. Kraehnert, H. Dau, P. Strasser, *J. Am. Chem. Soc.* **2017**, *139*, 2070.

[53] W. Ai, Z. Luo, J. Jiang, J. Zhu, Z. Du, Z. Fan, L. Xie, H. Zhang, W. Huang, T. Yu, *Adv. Mater.* **2014**, *26*, 6186.

[54] F. Hu, H. Yang, C. Wang, Y. Zhang, H. Lu, Q. Wang, *Small* **2017**, *13*, 160257.

[55] I. S. Amiinu, X. Liu, Z. Pu, W. Li, Q. Li, J. Zhang, H. Tang, H. Zhang, S. Mu, *Adv. Funct. Mater.* **2018**, *28*, 1704638.

[56] L. Zhong, J. O. Jensen, L. N. Cleemann, C. Pan, *Sci. Bull.* **2017**, *63*, 24.

[57] F. Meng, H. Zhong, D. Bao, J. Yan, X. Zhang, *J. Am. Chem. Soc.* **2016**, *138*, 10226.

[58] M. D. Meganathan, S. Mao, T. Huang, G. Sun, *J. Mater. Chem. A* **2017**, *5*, 2972.

[59] W. Yang, X. Liu, L. Chen, L. Liang, J. Jia, *Chem. Commun.* **2017**, *53*, 4034.

[60] S. Gadipelli, T. Zhao, S. A. Shevlin, Z. Guo, *Energy Environ. Sci.* **2016**, *9*, 1661.

[61] E. Fabbri, M. Nachtegaal, T. Binninger, X. Cheng, B.-J. Kim, J. Durst, F. Bozza, T. Graule, R. Schäublin, L. Wiles, M. Pertoso, N. Danilovic, K. E. Ayers, T. J. Schmidt, *Nat. Mater.* **2017**, *16*, 925.

[62] X. Zheng, B. Zhang, P. D. Luna, Y. Liang, R. Comin, O. Voznyy, L. Han, F. P. G. de Arquer, M. Liu, C. T. Dinh, T. Regier, J. J. Dynes, S. He, H. L. Xin, H. Peng, D. Prendergast, X. Du, E. H. Sargent, *Nat. Chem.* **2018**, *10*, 149.

[63] Z.-H. Xue, H. Su, Q.-Y. Yu, B. Zhang, H.-H. Wang, X.-H. Li, J.-S. Chen, *Adv. Energy Mater.* **2017**, *7*, 1602355.

[64] X. Yan, Y. Jia, J. Chen, Z. Zhu, X. Yao, *Adv. Mater.* **2016**, *28*, 8771.